# Solution Studies of Staphylococcal Nuclease H124L. 1. Backbone $^1H$ and $^{15}N$ Resonances and Secondary Structure of the Unligated Enzyme As Identified by Three-Dimensional NMR Spectroscopy[†,‡]

Jinfeng Wang, Ed S. Mooberry, William F. Walkenhorst, and John L. Markley*

*Biochemistry Department and National Magnetic Resonance Facility at Madison, College of Agricultural and Life Sciences, University of Wisconsin, 420 Henry Mall, Madison, Wisconsin 53706*

*Received June 4, 1991; Revised Manuscript Received September 20, 1991*

ABSTRACT: The backbone $^1H$ and $^{15}N$ resonances of unligated staphylococcal nuclease H124L (recombinant protein produced in *Escherichia coli* whose sequence is identical to the nuclease produced by the V8 strain of *Staphylococcus aureus*) have been assigned by three-dimensional (3D) $^1H$–$^{15}N$ NOESY-HMQC NMR spectroscopy at 14.1 tesla. The protein sample used in this study was labeled uniformly with $^{15}N$ to a level greater than 95% by growing the *E. coli* host on a medium containing [99% $^{15}N$]ammonium sulfate as the sole nitrogen source. The assignments include 82% of the backbone $^1H^N$ and $^1H^\alpha$ resonances as well as the $^{15}N$ resonances of non-proline residues. Secondary structural elements ($\alpha$-helices, $\beta$-sheets, reverse turns, and loops) were determined by analysis of patterns of NOE connectivities present in the 3D spectrum.

Heteronuclear three-dimensional NMR[1] techniques, which have been developed over the past three years (Fesik & Zuiderweg, 1990; Kay et al., 1991), offer a promising general approach for extensive assignments of resonances in proteins in the 15–30-kDa range. Various 3D NMR pulse sequences have been designed to exploit spin–spin coupling in proteins labeled uniformly with $^{13}C$ and/or $^{15}N$. One of these is the 3D analogue of the 2D $^1H$–$^{15}N$ HMQC-NOE experiment (Shon & Opella, 1989) that was used in the analysis of the (nuclease H124L)·pdTp·$Ca^{2+}$ ternary complex (Wang et al., 1990a). This 3D experiment, nuclear Overhauser–multiple-quantum coherence (NOESY-HMQC), has been used in conjunction with 3D Hartmann–Hahn multiple-quantum coherence (HOHAHA-HMQC) spectroscopy in the assignment of backbone $^{15}N$ and $^1H$ resonances of uniformly $^{15}N$-labeled proteins (Zuiderweg et al., 1989; Kay et al., 1989; Marion et al., 1989a,b). For example, backbone $^{15}N$ and $^1H$ resonances of interleukin-1$\beta$ (17.4 kDa) were assigned by combining NOESY-HMQC and HOHAHA-HMQC data (Driscoll et al., 1990a). Triple-resonance ($^1H$, $^{13}C$, $^{15}N$) 3D and 4D experiments have been used to obtain complete backbone, $^1H$, $^{13}C$, and $^{15}N$ assignments for calmodulin (16.7 kDa) (Ikura et al., 1990a) and to determine the complete side-chain assignments of interleukin-1$\beta$ (Clore et al., 1990a). 3D data also have been used in the analysis of protein solution structure (Driscoll et al., 1990b; Clore et al., 1990b).

Fairly complete $^1H$, $^{13}C$, and $^{15}N$ NMR assignments have been reported for two variants of staphylococcal nuclease complexed with a mononucleotide bisphosphate inhibitor (pdTp) and the metal ion required for catalytic activity ($Ca^{2+}$): Torchia et al. (1989) have studied the (nuclease wt)·pdTp·$Ca^{2+}$ ternary complex at pH 7.4, and our group has studied the (nuclease H124L)·pdTp·$Ca^{2+}$ ternary complex at pH 5.1 (Wang et al., 1990a,b). The next stage in developing an understanding of the structural changes that accompany complex formation in solution (Markley & Jardetzky, 1970) was to obtain similar assignments for the unligated enzyme.

We employed the following strategy in assigning the $^1H$, $^{13}C$, and $^{15}N$ NMR spectra of unligated nuclease H124L and comparing these results with those for the ternary complex: (1) Intraresidue spin systems were identified from homonuclear and heteronuclear 2D NMR experiments described in the accompanying paper (Wang et al., 1992). (2) The main-chain connectivities from these spin systems were then matched against 3D $^1H$–$^{15}N$ NOESY-HMQC data to provide sequential assignments for 82% of the main-chain $^1H^\alpha$, $^1H^N$, $^1H^\beta$, and $^{15}N$ resonances as described in the present paper. (3) Then the main-chain sequential assignments were refined by reference to the 2D data sets and extended out along the remainder of the side chains. (4) Finally, a quantitative analysis was made of the chemical shift changes that accompany in-

[†] This work was supported by Grant GM35976 from the National Institutes of Health (NIH). NMR studies were carried out in the National Magnetic Resonance Facility at Madison, which is supported by NIH Grant RR02301. Equipment in the NMR Facility was purchased with funds from the NIH Biomedical Research Technology Program, National Center for Research Resources (Grant RR02301), the University of Wisconsin, the National Science Foundation Biological Instrumentation Program (Grant DMB-8415048), NIH Shared Instrumentation Program (Grant RR02781), and the U.S. Department of Agriculture.

[‡] NMR data were deposited in BioMagResBank (Ulrich et al., 1989) under ref ID 956.

[1] Abbreviations: COSY, 2D correlated spectroscopy; DISNMR, spectral processing program for the Bruker Aspect 1000/3000 computer (1988 version); FID, free induction decay; HMQC, heteronuclear multiple-quantum correlation; HOHAHA, 2D $^1H$ homonuclear Hartmann–Hahn magnetization transfer spectroscopy; [na]H124L, nuclease H124L at natural abundance; [95% UL $^{15}N$]H124L, nuclease H124L enriched uniformly with $^{15}N$ to >95% isotope; NMR, nuclear magnetic resonance; NOE, nuclear Overhauser enhancement; NOESY, 2D NOE spectroscopy; nuclease wt, recombinant staphylococcal nuclease (EC 3.1.31.1) produced in *Escherichia coli* whose sequence is identical to the nuclease produced by the Foggi strain of *Staphylococcus aureus*; nuclease H124L, recombinant staphylococcal nuclease produced in *E. coli* whose sequence is identical to the nuclease produced by the V8 strain of *S. aureus* (its sequence differs from nuclease wt by the substitution of Leu for His at position 124); pdTp, thymidine 3′,5′-bisphosphate; pH*, pH meter reading (glass electrode calibrated with normal buffers) of a sample dissolved in $^2H_2O$ uncorrected for deuterium isotope effects; RCT-COSY, 2D relayed coherence transfer spectroscopy; TPPI, time-proportional phase incrementation; TSP, 3-(trimethylsilyl)propionate-$d_4$; UL, uniform label; 2D, two dimensional; 3D, three dimensional.

0006-2960/92/0431-911$03.00/0 

hibitor binding. Although the 3D data provided information for determining the sequential assignments and secondary structural features, they did not permit accurate chemical shift determinations owing to the poor digital resolution in the $\omega_1$, $\omega_2$, and $\omega_3$ dimensions. For this reason, accurate $^1H$, $^{13}C$, and $^{15}N$ chemical shifts were obtained from the 2D NMR spectra. Steps 3 and 4 are reported in the accompanying paper (Wang et al., 1992).

## Experimental Procedures

*Protein Samples.* Recombinant staphylococcal nuclease was prepared as described previously (Wang et al., 1990a,b). [99% $^{15}N$]Ammonium sulfate was used as the sole nitrogen source during growth. The purified nuclease H124L was enriched uniformly to >95% $^{15}N$ isotope. The protein solution used for 3D data collection contained 5 mM [95% UL $^{15}N$]H124L dissolved in 90% $H_2O$/10% $^2H_2O$ with 0.3 M KCl; the pH was 5.1. Samples were prepared as described for the nuclease H124L ternary complex (Wang et al., 1990a).

*3D NOESY-HMQC Experiment.* The principles and applications of the 3D NOESY-HMQC experiment have been described in detail (Kay et al., 1989; Zuiderweg et al., 1989). Three-dimensional $^1H$–$^{15}N$ NOESY-HMQC data were collected with a Bruker AM-600 spectrometer at a probe temperature of 45 °C. A modified NOESY-HMQC pulse sequence (Marion et al., 1989b) was used in acquiring the 3D data. A $10\,000^\circ_x$–$5000^\circ_y$ $^1H$ pulse was used in place of the first 90° pulse to achieve a "steady state" (Marion et al., 1989c). A single 180° pulse was used in place of WALTZ decoupling during the $t_1$ evolution period. DANTE-type presaturation (Morris et al., 1978) was applied for 1.0 s to suppress the water resonance. The $^1H$ carrier frequency was alternated between the water resonance (for presaturation) and the center of the amide proton region (for $^1H$ observation). The spectral width in the $\omega_3$ dimension (3623.3 Hz) was chosen to be just sufficient to cover the region from the $^1H^\alpha$ resonances downfield of water to the $^1H^N$ of Thr$^{120}$. The $H_2O$ resonance was at the right edge of the spectrum in $\omega_3$, and the $^{15}N$ carrier frequency was set at the center of the amide $^{15}N$ region (120 ppm). A sweep width of 2272.7 Hz was employed in $\omega_2$. The NOE mixing time was 120 ms. The 3D data matrix ($\omega_1 \times \omega_2 \times \omega_3$) contained 256 (real) × 64 (complex) × 512 (real) points. The acquisition times in $t_1$, $t_2$, and $t_3$ were 17.7, 7.0, and 70 ms, respectively; 16 scans were collected per $t_1$ increment. Two sets of data were collected in the $\omega_2$ dimension, and every third and fourth FID was negated to attain States–TPPI detection in $\omega_2$ (States et al., 1982; Simorre et al., 1990).

*3D NMR Data Processing.* The first step in processing the NOESY-HMQC NMR data (the $\omega_2$ Fourier transformation) was performed on a personal computer (American Megatrends, Inc., model 386) with a software routine (W2FFT) that makes use of an array processor board (Eighteen Eight Laboratories, model PL 800) [see Markley et al. (1991)]. Fourier transforms of the $\omega_1$–$\omega_3$ 2D planes were carried out subsequently on a Bruker Aspect 1000 data station; a simple DISNMR macro was written to facilitate the computations. Zero-filling was applied before Fourier transformation. The data were apodized with a 90°-shifted sine bell function in $\omega_1$ and a 45°-shifted sine bell function in $\omega_3$. No baseline correction was used afterward. Phase corrections were calculated and applied as described by Kay et al. (1989). The data size after transformation was 1024 × 64 × 1024 points ($\omega_1 \times \omega_2 \times \omega_3$), and the digital resolution was 14.15, 35.5, and 7.08 Hz/point for $\omega_1$, $\omega_2$, and $\omega_3$, respectively. Data transfers between the Bruker Aspect 1000 and the personal computer was by ZZNET (Zolnai et al., 1990).

$^1H$ chemical shifts in the $^1H$–$^1H^N$ slices through the 3D data were calibrated by assigning the clearly resolved E101 $^1H^N$ diagonal peak a chemical shift value of 6.17 ppm. This value was obtained by measuring the $^1H$ chemical shift of E101 relative to internal TSP in the 1D $^1H$ NMR spectrum of [na]H124L. The $^{15}N$ chemical shift scale was calibrated by assigning the E101 $^{15}N$ peak a value (113.5 ppm) equal to that determined previously from a 2D HMQC-NOE experiment (Wang et al., 1992); $^{15}N$ chemical shifts are reported relative to the signal of liquid ammonia.

*Assignment Pathway in the 3D $^1H$–$^{15}N$ Heteronuclear NOESY-HMQC Spectrum.* The 3D $^1H$–$^{15}N$ NOESY-HMQC spectrum is viewed as a series of 2D $^1H$–$^1H^N$ NOESY planes (in $\omega_1$–$\omega_3$) edited by the chemical shift of the $^{15}N_i$ atom (in $\omega_2$) directly bonded to the $^1H^N_i$ (Figure 1). The full $^1H$ spectrum is recorded in the $\omega_1$ dimension, amide nitrogen resonances are recorded in the $\omega_2$ dimension, and the $^1H^N$ region is recorded in the $\omega_3$ dimension. In the 3D $^1H$–$^{15}N$ NOESY-HMQC NMR spectrum, the sequential connectivity between one residue and the next usually joins two separate $^1H$–$^1H^N$ NOESY planes, unless the $^{15}N$ chemical shifts of the two residues are similar. Projection of the 3D spectrum along $\omega_2$ gives the $^1H$–$^1H^N$ region of the standard 2D $^1H$–$^1H$ NOESY ($H_2O$) spectrum. A similar projection of $^1H^{\alpha,\beta}_i$–$^1H^N_{i+1}$ or $^1H^N_i$–$^1H^N_{i+1}$ sequential walks through the 3D data yields the sequential NOE connectivities observed in a standard NOESY ($H_2O$) spectrum. Therefore, all the criteria that have been developed for the determination of $\alpha$-helix and $\beta$-sheet in 2D NOESY spectra (Wagner et al., 1986; Wand et al., 1986) are applicable to the 3D $^1H$–$^{15}N$ NMR data.

Figure 1A is a schematic representation of $^1H^\alpha_i$–$^1H^N_{i+1}$ (or $^1H^\beta_i$–$^1H^N_{i+1}$) sequential connectivities in the 3D spectrum. The $^1H^\alpha_i$–$^1H^N_{i+1}$ sequential walk can be represented conveniently by drawing connectivities in a series of ordered $^1H$–$^1H^N$ strips (Figure 1A, bottom). Figure 1B is a schematic representation of $^1H^N_i$–$^1H^N_{i+1}$ ($d_{NN}$) sequential connectivities. $^1H^N_i$–$^1H^N_{i+1}$ NOE cross peaks are located in both the $i$th and the ($i$+1)th $^1H$–$^1H^N$ slices on opposite sides of the diagonal. Projection of the combined triangles gives the characteristic $^1H^N_i$–$^1H^N_{i+1}$ rectangle found in 2D $^1H$–$^1H$ NOESY data. In the sequential walk from residue $i$ to residue $i$+2, two interresidue NOE cross peaks should be found along the $\omega_1$ axis of the ($i$+1)th plane at the $^1H^N_{i+1}$ chemical shift: $^1H^N_i$–$^1H^N_{i+1}$ and $^1H^N_{i+1}$–$^1H^N_{i+2}$. These two cross peaks define triangles whose symmetrical images are found in the $i$th and ($i$+2)th slices, respectively. The $^1H^N_i$–$^1H^N_{i+1}$ sequential walk starts from $^1H^N_i$ diagonal peak in $i$th plane, passes through the $^1H^N_i$–$^1H^N_{i+1}$ interresidue NOE cross peak, and ends at the $^1H^N_{i+1}$ diagonal peak in the ($i$+1)th plane. When the inter- and intraresidue NOE cross peaks in sequentially ordered strips are connected by lines, one obtains a series of linked rectangles (Figure 1B, bottom). Linked diagonals through the adjacent rectangles trace out the sequential ($^1H^N$–$^{15}N$–$^1H^N$) 3D cross peaks.

Secondary structural features can be recognized from the patterns of NOE connectivities in sequentially ordered slices. For example, $^1H^N_i$–$^1H^N_{i+2}$ NOE connectivities from $\alpha$-helical regions are weak and are not observed in the 3D slices. Thus the $d_{NN}$ sequential connectivities from an $\alpha$-helix give a pattern of rectangles in series without any overlap (as shown at the bottom of Figure 1B). Reverse turns give rise to only a few rectangles that may overlap. Antiparallel $\beta$-pleated sheet, by contrast, gives discrete rectangles with one rectangle covering another in the $\omega_3$ dimension.

In determining sequential assignments from a 3D $^1H$–$^{15}N$ NOESY-HMQC spectrum, it is helpful to have additional

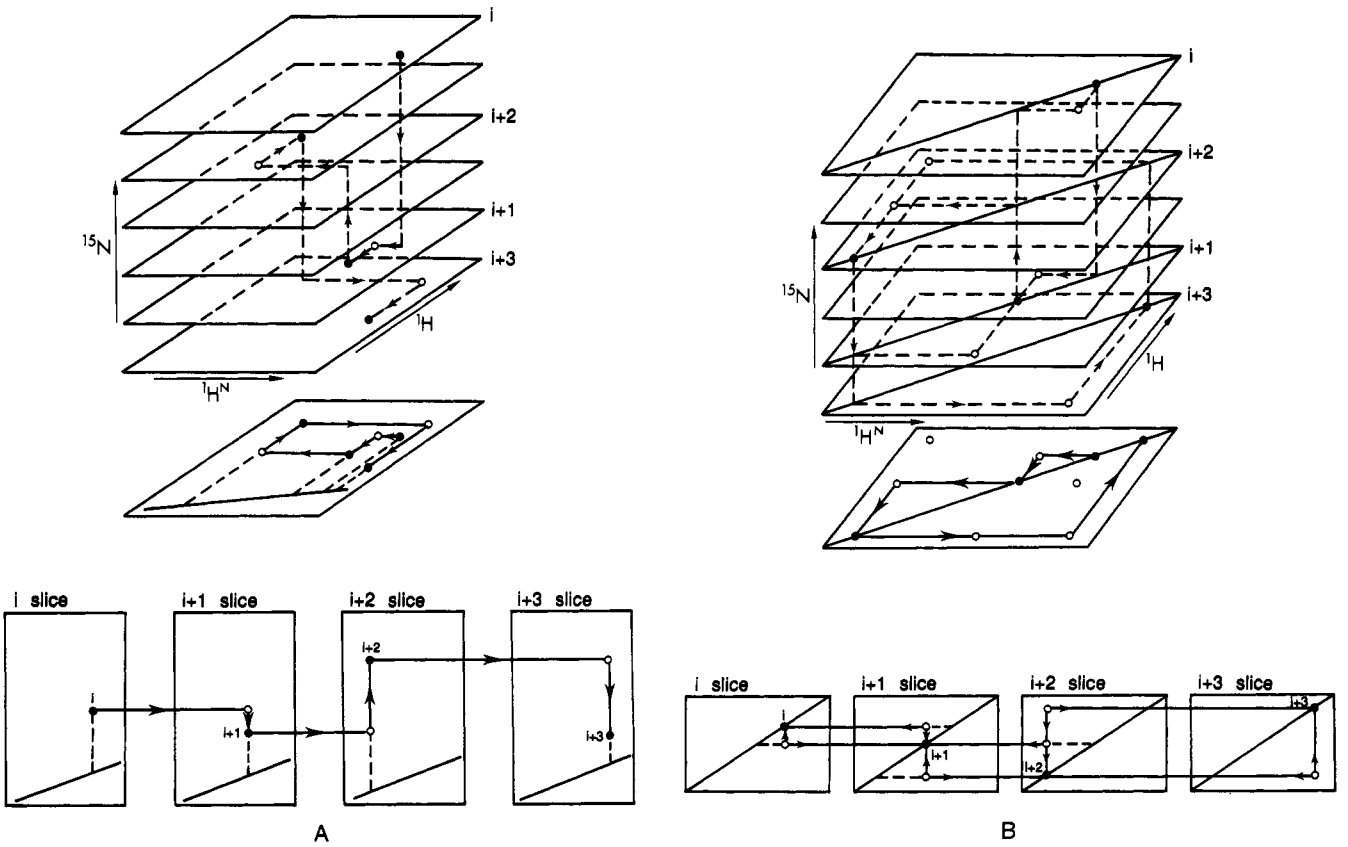


FIGURE 1: (A) Schematic representation of the $d_{\alpha N}$ sequential connectivities in a 3D $^1$H–$^{15}$N NOESY-HMQC spectrum. (Top) Three-dimensional view. The vertical arrows indicate the sequential pathway of $^{15}$N resonances. The arrows within the $^1$H–$^1$H$^N$ slices follow sequential connectivities that link $^1$H$^{\alpha}_i$ and $^1$H$^N_{i+1}$. (Middle) Projection of the sequential pathway in the 3D $^1$H–$^1$H$^N$ slices onto the $^1$H–$^1$H$^N$ plane gives a pattern identical to the sequential walk obtained by analyzing a conventional 2D $^1$H–$^1$H NOESY ($H_2O$) spectrum. (Bottom) Selected 3D $^1$H–$^1$H$^N$ slices arranged in sequential order. The $d_{\alpha N}$ walk is shown by solid lines with arrows. Intraresidue NOE cross peaks are represented by dots, and interresidue NOE cross peaks are represented by circles. (B) Schematic view of the $d_{NN}$ connectivities in a 3D $^1$H–$^{15}$N NOESY-HMQC spectrum. (Top) Three-dimensional view. The arrows illustrate the sequential pathway of the connected amide protons. The $d_{NN}$ NOE cross peaks appear as symmetry-related triangles on either side of the sequential $^1$H–$^1$H$^N$ slices along the diagonal. (Middle) Projection of the linked 3D peaks onto the $^1$H–$^1$H$^N$ plane yields a pattern equivalent to the $d_{NN}$ walk obtained by analyzing a conventional 2D $^1$H–$^1$H NOESY ($H_2O$) spectrum. (Bottom) Selected slices arranged in sequential order. The solid lines with arrows trace out the NOE connectivity pattern between amide protons in consecutive slices. The diagonal peaks are represented by dots. The NOE cross peaks are represented by circles.

data that distinguish intraresidue and interresidue NOE cross peaks. Marion et al. (1989a) used 3D HOHAHA-HMQC data for this purpose. Although we collected a 3D HOHAHA-HMQC spectrum of nuclease H124L (not shown), it was of poor quality. Information about through-bond connectivities was obtained instead from RCT-COSY ($H_2O$) data (not shown) and from the 2D data sets described in the accompanying paper (Wang et al., 1992).

All 64 of the $^1$H–$^1$H$^N$ slices of the 3D $^1$H–$^{15}$N NOESY-HMQC spectrum were plotted at the same contour levels by using a DISNMR macro on an Aspect 1000 computer to drive a Hewlett Packard model 7550A plotter. Because of the relatively poor digital resolution in the $\omega_2$ dimension, cross peaks from each amide proton were found in more than one $^1$H–$^1$H$^N$ slice and with some variation in peak position. For this reason, neighboring slices had to be examined in order to determine the correct position of the 3D cross peaks. The criterion used was to pick the slice that had the highest aggregate intensity for the peaks assigned to the selected amino acid residue. Of the 64 $^1$H–$^1$H$^N$ slices, 39 were selected for further analysis. In each strip, all the inter- and intraresidue NOE's arising from the $^1$H$^N$ of the selected residue appear along the $\omega_1$ dimension. Baseplane distortions led to the loss of some peaks in the contour plots of these slices. The missing peaks (represented by small boxes in the figures) were detected in cross sections of the $^1$H–$^1$H$^N$ slice taken along the $\omega_1$ dimension. The sequential order of the $^1$H–$^1$H$^N$ strips was determined by matching interresidue NOE connectivities; then the ordered strips were plotted with the DISNMR program. The width of each plotted strip was about 0.16 ppm (0.08 ppm to either side of the $^1$H$^N_i$ chemical shift).

## Results and Discussion

Strips were extracted from selected 2D slices of the 3D $^1$H–$^{15}$N NOESY-HMQC spectrum at positions that contained patterns of cross peaks indicative of sequential assignments and secondary structure. These strips were then aligned sequentially by analyzing the interresidue NOE connectivities. The patterns of cross peaks in the ordered strips are diagnostic of different kinds of secondary structure as mentioned above.

### *Assignment of α-Helical Segments*

Sequences of nonoverlapping rectangles found in the $d_{NN}$ connectivity pattern established the sequential assignments for three $\alpha$-helical stretches without reference to spin system characterization or the peptide sequence. The polarity of each stretch was established by analysis of spin systems or by reference to $d_{\alpha N}$ or $d_{\beta N}$ sequential walks, which are directional. Segments of $\alpha$-helix are expected to produce strong intraresidue $^1$H$^{\beta}_i$–$^1$H$^N_i$ and interresidue $^1$H$^{\beta}_i$–$^1$H$^N_{i+1}$ NOE's (Englander et al., 1987). Figure 2 summarizes the observed NOE's from the three $\alpha$-helices described in detail below.

*(1) Val$^{99}$ to Ala$^{109}$.* Two $^1$H$^N_i$–$^1$H$^N_{i+1}$ NOE cross peaks ($\omega_1$ = 7.87 and 9.68 ppm, Figure 3) appear downfield of the

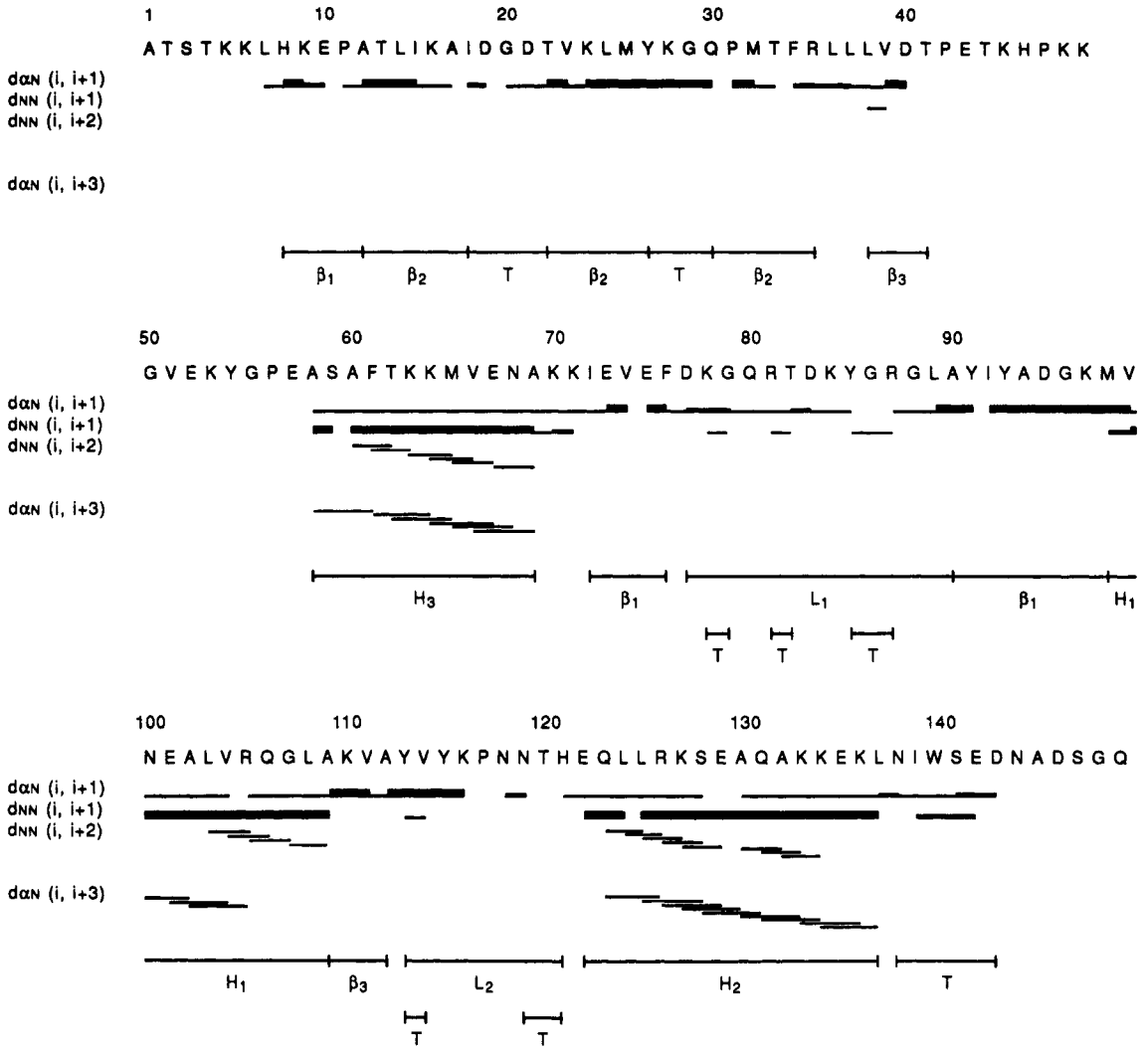


FIGURE 2: Amino acid sequence of staphylococcal nuclease H124L together with a summary of the location of secondary structural features determined from the NMR results. Nearest-neighbor $d_{\alpha N}$ and $d_{NN}$ NOE connectivities and long-range $d_{NN}(i,i+2)$ and $d_{\alpha N}(i,i+3)$ connectivities are indicated by bars. The $d_{NN}(i,i+2)$ connectivities are exclusively from the 2D NOESY data (Wang et al., 1992); all other NOE connectivities are from combined 2D and 3D data. The thickness of the bars denotes whether the NOE's are strong (thick), medium (medium), or weak (thin line). Location of secondary structural elements are indicated by symbols: H, $\alpha$-helix; T, turn; L, loop; $\beta$, antiparallel $\beta$-sheet.

diagonal (6.17 ppm) in the strip assigned to E101: that at $\omega_1$ = 7.87 ppm arises from the interresidue NOE between the $^1H^N$'s of A102 (7.87 ppm) and E101 (6.17 ppm); that at $\omega_2$ = 9.68 ppm arises from the NOE between the $^1H^N$ of N100 (9.68 ppm) and the $^1H^N$ of E101. The cross peak at $\omega_1$ = 7.87 ppm connects the diagonal peak from E101 (6.17 ppm) with the diagonal peak from A102 (7.87), and its image cross peak at $\omega_1$ = 6.17 ppm in the A102 strip connects the diagonal peak from A102 (7.87 ppm) with the diagonal peak from E101 (6.17 ppm). These four peaks form a rectangular connectivity pattern. The same pattern is shown by the diagonal peaks of E101 and N100 (9.68 ppm) and the image NOE cross peaks at $\omega_1$ = 9.68 ppm and 6.17 ppm in the E101 and N100 strips, respectively. These two rectangles are linked but do not overlap one another. The A102 strip contains an additional interresidue NOE cross peak at $\omega_1$ = 8.05 ppm which connects the diagonal peak in the A102 strip to the diagonal peak in the L103 strip. By continuing this pattern, the $d_{NN}$ sequential assignments were extended from V99 to A109.

The polarity of the stretch was confirmed by the $d_{\beta N}$ sequential walk indicated by solid lines with arrows in Figure 3, which is broken at G107. Although an $\alpha$-helix produces sequential $d_{\alpha N}$ connectivities that are weaker than $d_{\beta N}$ connectivities, the $d_{\alpha N}$ sequential walk for this stretch is clearly visible (Figure 3). The geometrical arrangement of atoms in an $\alpha$-helix also leads to the observation of interresidue $d_{\alpha N}(i,i+3)$ and $d_{\alpha N}(i,i+4)$ connectivities (Wagner et al., 1986; Englander et al., 1987). The V104 strip contains a $^1H^{\alpha}_{i-3}$–$^1H^N_i$ connectivity to E101 and a $^1H^{\alpha}_{i-4}$–$^1H^N_i$ connectivity to N100. NOE connectivities are observed between the $^1H^{\alpha}$ of V99 and the $^1H^N$'s of A102 and L103 in their respective strips.

(*2*) *Glu*[122] *to Leu*[137]. Figure 4 shows a series of 15 $d_{NN}$ rectangular connectivities assigned to the $\alpha$-helix spanning residues E122–L137. Because the interresidue cross peaks of Q131, E135, and K136 have similar chemical shifts, the corresponding strips show only a single overlapped peak near the diagonal. These strips were assigned by noting that every diagonal peak from residues in an $\alpha$-helix is flanked by $^1H^N$ NOE cross peaks to both of the adjacent strips at the same $\omega_1$ chemical shift. For example, the diagonal peak in the Q131 strip at $\omega_1$ = 7.56 ppm is flanked by cross peaks at this chemical shift in the A130 and A132 strips (Figure 4). Therefore, each of the two overlapped $d_{NN}$ cross peaks in the Q131 strip lines up separately with the diagonal peaks from A130 and A132. The overlapped $d_{NN}$ cross peaks in the E135 and K136 strips were analyzed in similar fashion. Only one of the symmetry-related $^1H^N$ NOE cross peaks between L124 and L125 was observed in the strips from these residues.

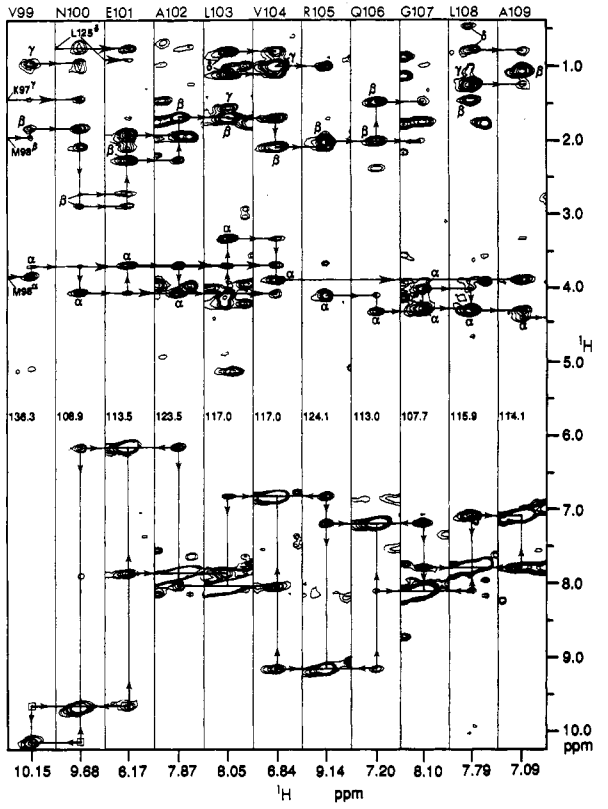


FIGURE 3: Series of strips selected from $^1$H–$^1$H$^N$ slices of the 3D $^1$H–$^{15}$N NOESY-HMQC spectrum. The strips have been arranged in sequential order. Each strip corresponds to one residue in the V99–A109 $\alpha$-helix. Because of poor resolution along the $^{15}$N dimension, some strips show cross peaks from other residues with similar $^{15}$N chemical shifts in addition to the NOE cross peaks of the selected residue. The assignment of each strip is given at the top by residue number and one-letter amino acid code. Identified intraresidue NOE cross peaks between side-chain protons and amide protons are indicated by Greek letters. Solid vertical lines with arrows denote NOE connectivities to the $^1$H$^N$ of the residue whose amide $^{15}$N is selected. Horizontal lines with arrows indicate NOE's from protons on adjacent residues. The vertical axis gives the $^1$H chemical shifts in ppm. The $^1$H$^N$ chemical shift (in ppm) of the selected residue is marked on the horizontal axis of each strip. The approximate $^{15}$N chemical shift of the slice from which the strip was taken is noted in each strip. The $^1$H$^N$ chemical shift values used here are the more accurate ones taken from the 2D NOESY data (Wang et al., 1992).

Apparently, the $d_{NN}$ cross peak in the L125 strip ($\omega_1$ = 7.78 ppm) lines up with the diagonal peak in the L124 strip, and the $d_{NN}$ cross peak in the L124 strip ($\omega_1$ = 7.84 ppm) lines up with the diagonal peak in the L125 strip. The chemical shift difference between these two resonances (0.06 ppm) was insufficient to permit resolution of the cross peak from the diagonal.

The $d_{\beta N}$ sequential walk from E122 to L137 is indicated in Figure 4. Besides the stretch of $d_{\alpha N}$ sequential connectivities, the $^1$H$^\alpha$ region contains several characteristic $d_{\alpha N}(i,i+3)$ and $d_{\alpha N}(i,i+4)$ NOE connectivities. In Figure 4, solid lines with arrows mark the $d_{\alpha N}(i,i+3)$ NOE's between the $^1$H$^\alpha$'s of L125, R126, K127, S128, A130, and K133 and the $^1$H$^N$'s of S128, E129, A130, Q131, K133, and K136, respectively. Indicated as well are the $d_{\alpha N}(i,i+4)$ NOE's between the $^1$H$^\alpha$'s of K127 and A130 and the $^1$H$^N$'s of Q131 and K134, respectively. All of these NOE's confirm the $\alpha$-helical nature of the E122–L137 segment as is summarized in Figure 2.

*(3) Ala$^{58}$ to Ala$^{69}$.* Figure 5 shows the data used for sequential assignment of the $\alpha$-helical segment from A58 to A69. The $d_{NN}$ sequential connectivities are represented by a series of 11 rectangles. NOE connectivities were not observed between the $^1$H$^N$ of A60 and the $^1$H$^N$'s of S59 and F61. The A60 resonance is found in a crowded part of the 2D $^1$H COSY ($H_2O$) fingerprint region (Wang et al., 1992). Since S59 shows only a single cross peak with A58, and F61 shows only a single cross peak with T62, their cross peaks to A60 must be located in the diagonal. This implies that the $^1$H$^N$ of A60 should be at either 8.21 ± 0.04 ppm or 8.26 ± 0.04 ppm. On searching these amide proton regions, $d_{\beta N}$ and $d_{\alpha N}$ NOE connectivities from S59 to F61 were identified, which assigned the $^1$H$^N$ resonance of A60 (8.18 ppm).[2]

The 3D $d_{\alpha N}$ and $d_{\beta N}$ sequential walks observed for the A58–A69 helix are indicated in Figure 5 by solid lines and arrows. A weak cross peak in the A69 strip ($\omega_1$ = 4.16 ppm) corresponds to the $d_{\alpha N}(i-3,i)$ NOE connectivity with residue V66. Similarly, $d_{\alpha N}(i,i+3)$ connectivities were found between A58 and F61 and between M65 and N68, and a $d_{\alpha N}(i,i+4)$ NOE connectivity was found between F61 and M65. It appears that the side chain of V66 extends toward the axis of the $\alpha$-helix, since the $^1$H$^\gamma$'s of V66 show strong NOE's with the $^1$H$^N$ of E67 and weak NOE's with the $^1$H$^N$'s of N68 and A69 (Figure 5).

### *Assignment of Antiparallel β-Sheets*

Antiparallel $\beta$-sheets are characterized by strong sequential $d_{\alpha N}$ NOE connectivities and $d_{\alpha N}(i,j+1)$ or $d_{\alpha N}(j,i+1)$ NOE connectivities between adjacent segments (Englander et al., 1987). In the 3D $^1$H–$^{15}$N NOESY-HMQC spectrum, the $d_{NN}(i-1,j+1)$ or $d_{NN}(j-1,i+1)$ NOE's between pairs of residues located in adjacent strands of the $\beta$-sheet should appear as a number of discrete rectangles. Reverse turns are formed by a short stretch of amino acid residues (usually four). A reverse turn should reveal itself in the 3D data as several rectangles (possibly overlapped) that connect the amide protons of four to five residues. Figure 6 shows a schematic representations of the $\beta$-structure and turns deduced from the 3D NMR data described below and the 2D NMR data presented in the following paper (Wang et al., 1992).

*(1) His$^8$ to Ala$^{12}$, Ile$^{72}$ to Phe$^{76}$, and Ala$^{90}$ to Val$^{99}$.* Strips corresponding to 19 residues were arranged next to one another in three sequential sets (Figure 7). Sequential $d_{\alpha N}$ NOE connectivities continue from A90 to V99 and then link up with the N-terminus of the V99–A109 $\alpha$-helix (Figure 3). Because the intraresidue NOE cross peak between the $^1$H$^\alpha$ and $^1$H$^N$ of Y91 is missing, no $d_{\alpha N}(i,i+1)$ NOE connectivity is observed between Y91 and I92. However, the Y91 strip, the $^1$H$^N$ of Y91 shows strong $d_{\alpha N}(i-1,i)$ NOE cross peaks with the $^1$H$^\alpha$ and $^1$H$^\beta$ of A90. In turn, the $^1$H$^N$ of A90 shows a strong $d_{\alpha N}(i-1,i)$ NOE cross peak with the $^1$H$^\alpha$ of L89, which is the C-terminal residue of the D77-L89 loop (described below). These sequential NOE's confirm the ordering of the A90–V99 strips shown in Figure 7.

The $d_{\alpha N}$ sequential walk through the middle five strips (Figure 7) continues from the dipeptide K70–K71, since the continuous $d_{\alpha N}$ and $d_{NN}$ sequential walks from A69 to I72 were determined (Figure 1S, Supplementary Material). An NOE cross peak between the $^1$H$^N$'s of K70 and K71 suggests that the backbone of the A69–I72 segment is bent at the dipeptide K70–K71 (Figure 1S). Owing to the absence of an intraresidue $d_{\alpha N}(i,i)$ NOE cross peak from V74, the interresidue $d_{\alpha N}(i-1,i)$ NOE cross peak between the $^1$H$^N$ of E75 and the $^1$H$^\alpha$ of V74 cannot be observed in the E75 strip. Nevertheless,

[2] It should be possible to analyze the ambiguous NOE between the $^1$H$^N$'s of S59 and A60 (8.18 ppm) by application of the recently developed 3D $^1$H–$^{15}$N HMQC–($^1$H–$^1$H NOESY)–$^1$H–$^{15}$N HMQC experiment (Ikura et al., 1990b).

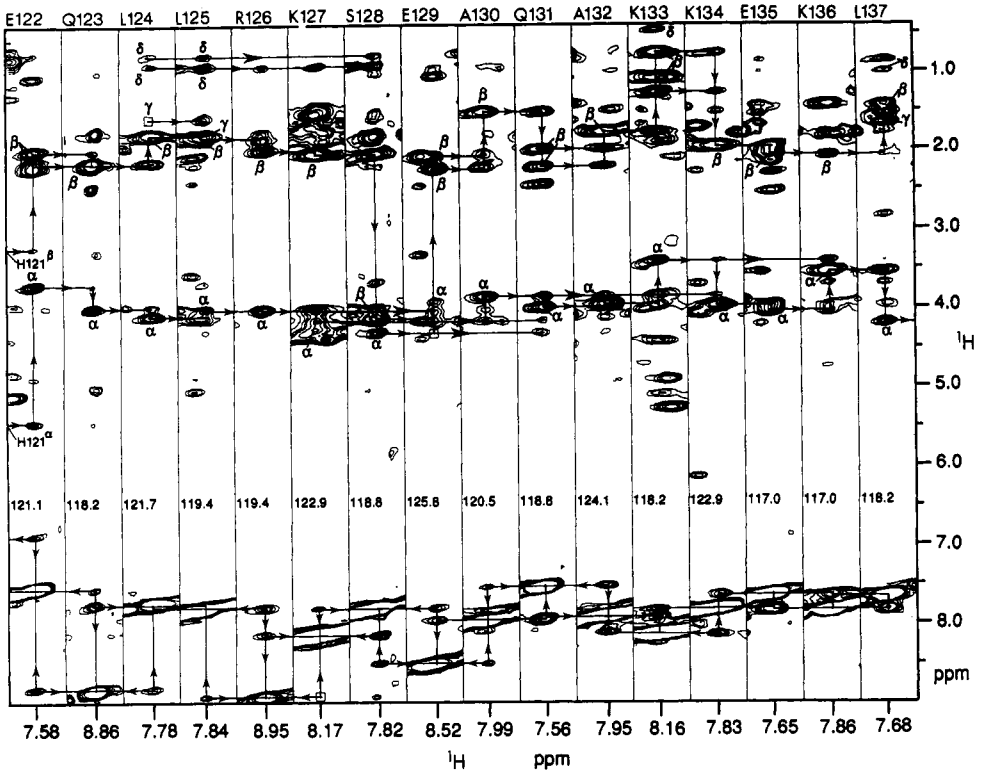


FIGURE 4: Combination of 16 $^1H$–$^1H^N$ strips selected from 3D NOESY-HMQC $^1H$–$^1H^N$ slices at different $^{15}N$ chemical shifts. The assigned strips were arranged according to the sequence of amino acid residues in the E122–L137 $\alpha$-helical segment. The sequential NOE connectivities in the $^1H^N$ and $^1H^\alpha/^1H^\beta$ regions are indicated by solid lines with arrows. The other notation is defined in the legend to Figure 3.

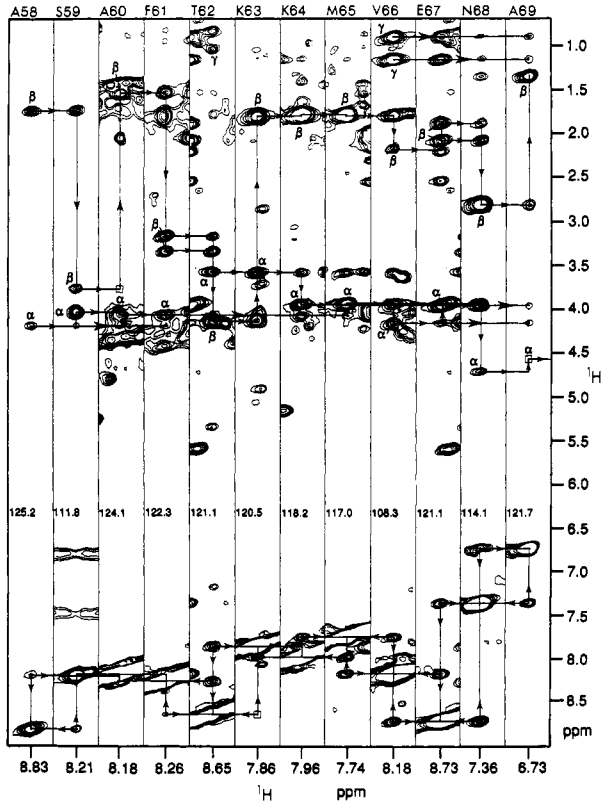


FIGURE 5: Combination of 12 $^1H$–$^1H^N$ strips assigned to amino acid residues in the $\alpha$-helical segment from A58 to A69. The sequential $d_{NN}$ connectivities and $d_{\alpha N}$,$d_{\beta N}$ sequential stretches are indicated. The notations are defined in the legend to Figure 3.

clearly resolved interresidue NOE cross peaks in the E75 strip between the $^1H^N$ of E75 and two $^1H^\gamma$'s and one $^1H^\beta$ of V74 provide convincing sequential connectivities between E75 and F76.

The first set of strips in Figure 7 includes those from H8, K9, E10, and A12 (residue 11 is a proline). The $d_{\alpha N}$ sequential walk in this segment starts from H8 and breaks at P11. The $d_{NN}(i-1,j+1)$ or $d_{NN}(i+1,j-1)$ rectangular connectivities that link H8 to F76 and E10 to V74 indicate that the two chains are antiparallel. The A12 strip contains an interresidue $d_{\alpha N}$ cross peak and a weak $d_{\beta N}$ cross peak between P11 and A12. The $^1H^\alpha$ of P11 shows a weak NOE with the $^1H^N$ of V74, and the $^1H^\alpha$ of E73 shows an NOE with the $^1H^N$ of A12 (Figure 7), which support the assignments in the H8–A12 segment of the antiparallel $\beta$-sheet.

Connectivities between pairs of $^1H^N$'s (A94 and K97, G96 and K97, and D95 and G96), which define three overlapping rectangles (Figure 7), reveal that A94–K97 forms a reverse turn. This is confirmed by NOE connectivities between the $^1H^\alpha$'s of A94 and D95 and the $^1H^N$'s of G96 and K97, respectively. NOE cross peaks between the $^1H^\alpha$ of M98 and the $^1H^N$ of A94 and between the $^1H^\alpha$ of Y93 and the $^1H^N$ of V99 locate residues M98 and V99 on one strand and residues Y93 and A94 on the adjacent strand of the antiparallel $\beta$-sheet.

Two long-range NOE rectangles (Figure 7) connect resonances assigned to the $^1H^N$'s of residues E73 and Y93 and residues E75 and Y91. In addition, NOE connectivities between the $^1H^\alpha$'s of F76, I92, and A94, and the $^1H^N$'s of Y91, E75, and E73, respectively, show unambiguously that I72–F76 and A90–A94 form two adjacent strands of antiparallel $\beta$-sheet.

The combined data (Figure 2) show that the three amino acid segments (H8–A12, I72–F76, and A90–V99) form an antiparallel $\beta$-sheet composed of four strands and one reverse turn as indicated schematically in Figure 6A.

*(2) Ala$^{12}$ to Arg$^{35}$.* A total of 22 strips selected from different $^1H$–$^1H^N$ slices of the 3D data are shown in Figure 8. The $d_{\alpha N}$ sequential walk starts from A12 and continues to K16. Spectral connectivity to A17 was provided by $d_{\beta N}(i-1,i)$ and $d_{NN}$ NOE's between K16 and A17. NOE's were observed

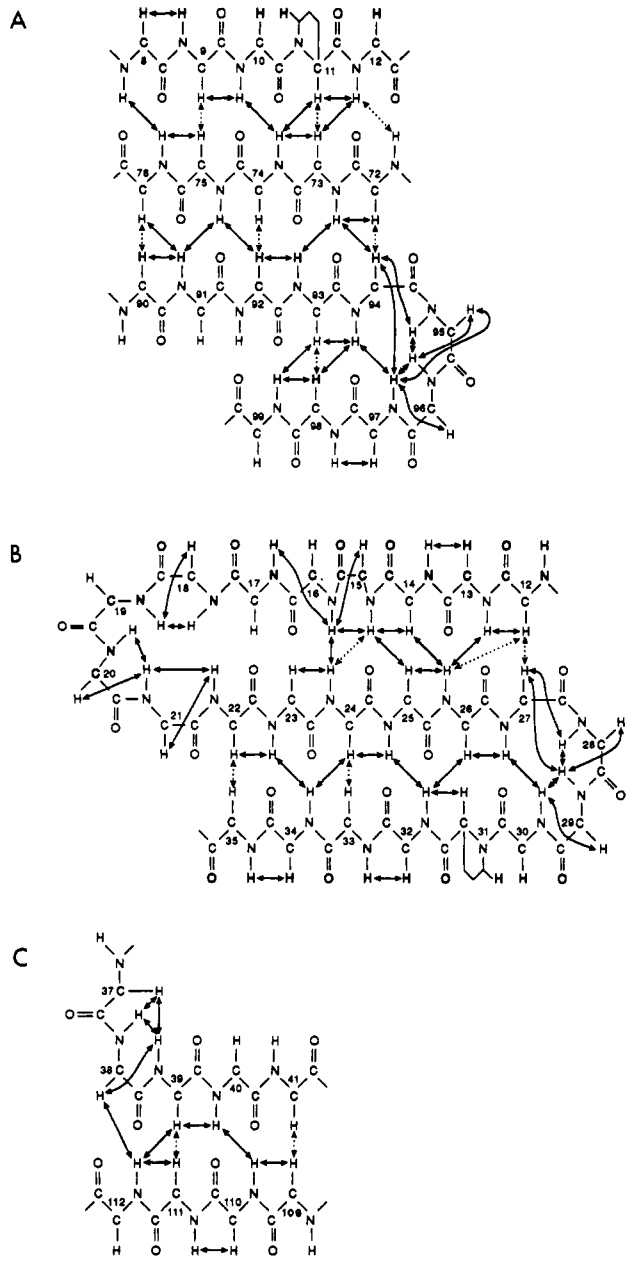

FIGURE 6: Schematic representation of three antiparallel $\beta$-sheets and turns of uncomplexed staphylococcal nuclease H124L. The assigned interstrand backbone NOE's and the sequential $d_{\alpha N}$ and short range $d_{NN}$ NOE's in the turns are denoted by double arrows. The solid arrows indicate NOE's detected in the present 3D NMR results; the dashed arrows represent NOE's detected in the 2D NMR studies (Wang et al., 1992).

between the $^1H^N$ of D19 and the $^1H^\alpha$ and $^1H^N$ of I18. Figure 8 shows 11 continuous $d_{\alpha N}$ sequential connectivities that include two glycine residues with an interval of eight residues between them. The only amino acid stretch in the nuclease H124L sequence that matches this is G20–Q30. The $^1H^\alpha$ and $^1H^\beta$'s of P31 show NOE's with the $^1H^N$ of M32. The $d_{\alpha N}$ sequential walk from P31 to R35 is interrupted between T33 and F34, because the T33 $d_{\alpha N}(i,i)$ intraresidue NOE was not observed. The assignments of I18, M32, and F34 were determined from 2D $^1H$ COSY, NOESY ($H_2O$), and 2D $^1H$-{$^{15}N$}HMQC-NOE data (Wang et al., 1992).

The presence of a reverse turn in the Y27–Q30 segment is indicated by the overlapping rectangular connectivities between $^1H^N$'s from three residue pairs, Y27 and Q30, K28 and G29, and G29 and Q30, and the NOE between the $^1H^\alpha$ of Y27 and the $^1H^N$ of G29 (Figure 8). Additional NOE's are observed between pairs of amino acids that surround the Y27–Q30 reverse turn: $^1H^N$–$^1H^N$ NOE connectivities between V23 and F34 and between L25 and M32 are revealed by discrete NOE rectangles (outlined by solid lines in Figure 8); additional NOE's link the $^1H^\alpha$'s of K24 and M26 with the $^1H^N$'s of F34 and M32, respectively (Figure 8). These data clearly show that P31–R35 and V23–M26 from adjacent strands of antiparallel $\beta$-sheet.

Figure 8 shows NOE connectivities between the $^1H^\alpha$'s of L14 and L25 and the $^1H^N$'s of M26 and I15, respectively. Two discrete NOE rectangles indicate the presence of NOE connectivities that link the $^1H^N$'s of T13 with M26 and K16 with K24. These show that the A12–A17 segment is located adjacent to the V23–M26 strand in an antiparallel $\beta$-sheet. This being so, the NOE connectivities shown by three sequential $^1H^N$ pairs, I18 and D19, G20 and D21, and D21 and T22, are indicative of an unusual $\alpha$-helical type turn that links two strands of the antiparallel $\beta$-sheet. The strong NOE between the $^1H^N$'s of I15 and K16 and the weak NOE between the $^1H^N$'s of K16 and A17 indicate that the A12–A17 strand is distorted around amino acids I15 and K16.

The NOE connectivities in the A12–R35 segment described above (Figure 2) reveal its structure as an antiparallel $\beta$-sheet consisting of three strands and two turns as shown schematically in Figure 6B.

(*3*) *Leu*$^{38}$ *to Thr*$^{41}$ *and Ala*$^{109}$ *to Ala*$^{112}$. Figure 9 combines the 3D $^1H$–$^1H^N$ strips corresponding to these two segments. Each individual segment is linked by $d_{\alpha N}$ sequential connectivities: the first starts from the $^1H^\alpha$ of R35, and the second starts from the $^1H^\alpha$ of L108. The two segments were aligned in the sequence by reference to their spin system types. The solid lines with arrows in Figure 9 indicate NOE's between the $^1H^N$'s of D40 and K110 and NOE's that link the $^1H^\alpha$'s of L38 and V39 with the $^1H^N$ of A112. A broken arrow in Figure 6C indicates the NOE between the $^1H^\alpha$'s T41 and A109 that was observed in 2D NMR spectra (Wang et al., 1992). These NOE's locate amino acid residues L39–T41 in one strand and A109–A112 in the adjacent strand of antiparallel $\beta$-sheet. Other NOE's shown in Figure 9 are the $^1H^N_i$–$^1H^N_{i+1}$ connectivity between L38 and V39, the $^1H^\alpha_i$–$^1H^N_{i+1}$ connectivity between L37 and L38, and the connectivities that link the $^1H^\alpha$'s of L37 and L38 with the $^1H^N$ of V39. These NOE's indicate the presence of a bend at the beginning of the L38–T41 strand.

### *Assignment of Loops and Turns*

All the NOE data pertinent to the loops and turns described below are summarized in Figure 2.

(*1*) *Big Loop*: *Asp*$^{77}$ *to Ala*$^{90}$. The 14 sequentially related strips assigned to this stretch are shown in Figure 10. The $d_{\alpha N}$ sequential walk starting from F76 is interrupted at D77–K78 and again at Y85–G86–R87. The K78 strip contains a diagonal peak but no intra- or interresidue cross peaks. K78 was assigned by interresidue $d_{\alpha N}(i-1,i)$, $d_{\beta N}(i-1,i)$, and $d_{NN}(i-1,i)$ NOE cross peaks in the G79 strip. G79 itself is clearly identified in the 3D spectrum by two intraresidue $d_{\alpha N}(i,i)$ cross peaks. In the other interrupted section (Y85–G86–R87), G86 shows $d_{NN}$ NOE connectivities in series with Y85 and R87. This pattern of NOE's indicates that Y85–G86–R87 forms an $\alpha$-helical turn. G88 was assigned on the basis of two intraresidue $d_{\alpha N}(i,i)$ cross peaks in the G88 strip and two interresidue $d_{\alpha N}(i-1,i)$ NOE cross peaks in the L89 strip.

The $d_{NN}$ NOE connectivities that link K78 with G79 and R81 with T82 (Figure 10) are consistent with bends at these positions. A long-range NOE between the $^1H^\alpha$ of T82 and

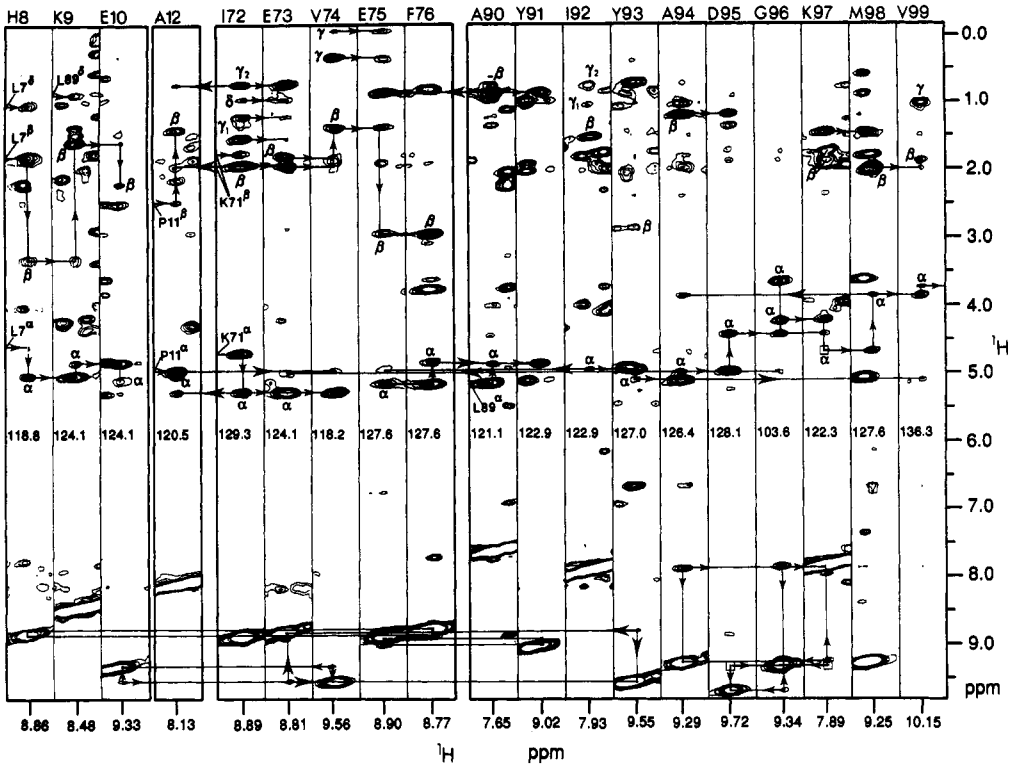


FIGURE 7: 3D NOE connectivities of the antiparallel $\beta$-sheet formed by segments H8–A12, I72–F76, and A90–V99. The missing strip corresponds to P11. All identified proton NOE connectivities are indicated by solid lines and arrows. The other notation is defined in the legend to Figure 3.

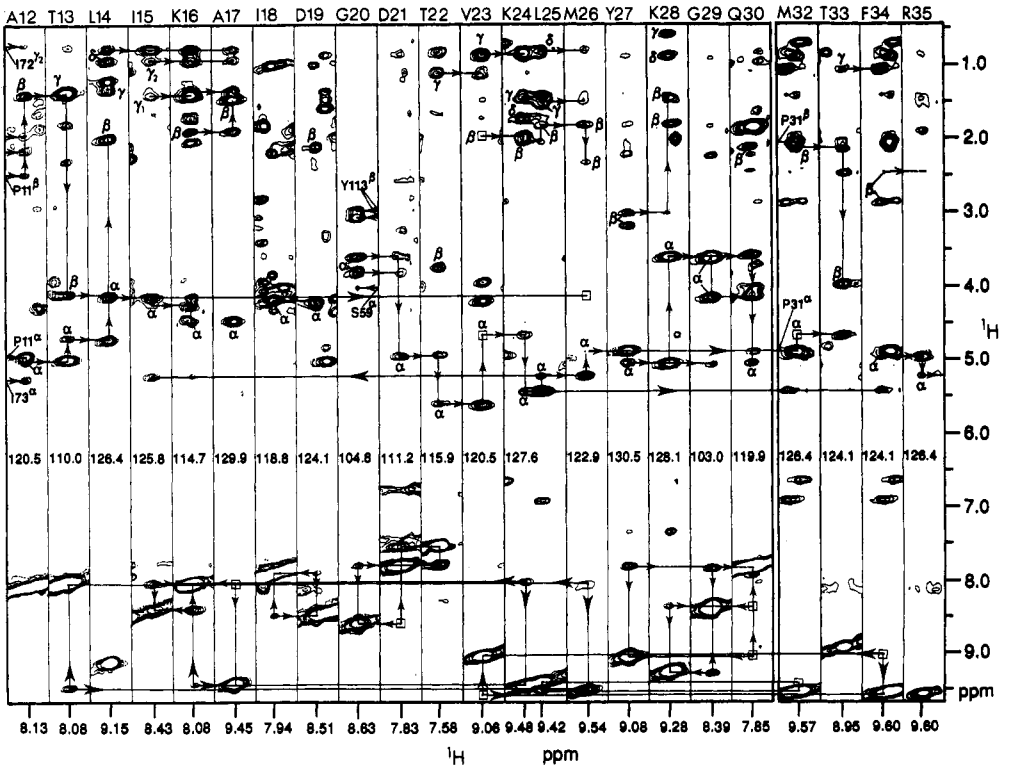


FIGURE 8: Combination of 20 $^1$H–$^1$H$^N$ strips selected from 3D $^1$H–$^1$H$^N$ slices that represent the antiparallel $\beta$-pleated sheet involving the segment from A12 to R35. The absent slice corresponds to P31. All identified sequential and long-range NOE connectivities are shown by solid lines and arrows. The other notation is defined in the legend to Figure 3.

the $^1$H$^N$ of L89 illustrates that the backbone of Q80–R81–T82–D83 bends toward the C-terminus of the D77–A90 segment.

(*2*) *Small Loop and α-Helical Turn.* The Y113–N119 segment forms a small loop that connects the carboxyl terminus of the A109–A112 $\beta$-sheet to the amino terminus of the E122–L137 $\alpha$-helix. Long-range NOE's between the $^1$H$^\alpha$ of K116 and the $^1$H$^N$'s of N118 and N119 indicate that K116–P117–N118–N119 forms a tight turn, and a $d_{NN}$ NOE between Y113 and V114 suggests the presence of an additional bend in the Y113–N119 segment (Figure 2S). The N138–D143 segment, near the carboxyl terminus, forms an $\alpha$-helical

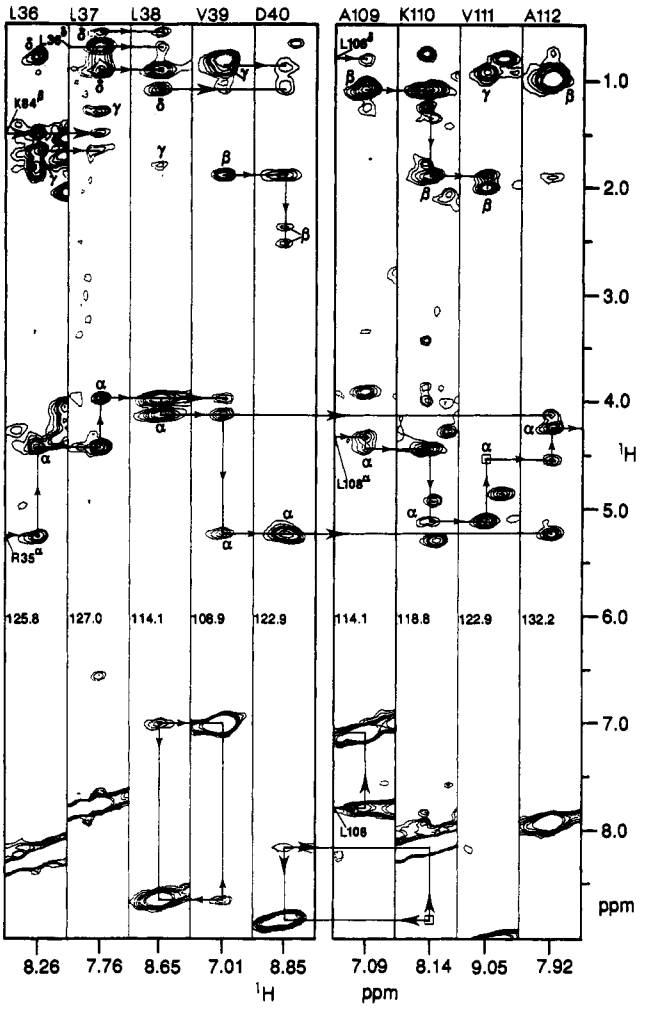


FIGURE 9: Selected set of $^1H$–$^1H^N$ strips that illustrate a small piece of antiparallel $\beta$-sheet made up of segments L38–T41 and A109–A112. The NOE connectivities in the amide and aliphatic regions are indicated by solid lines with arrows. The other notation is defined in the legend to Figure 3.

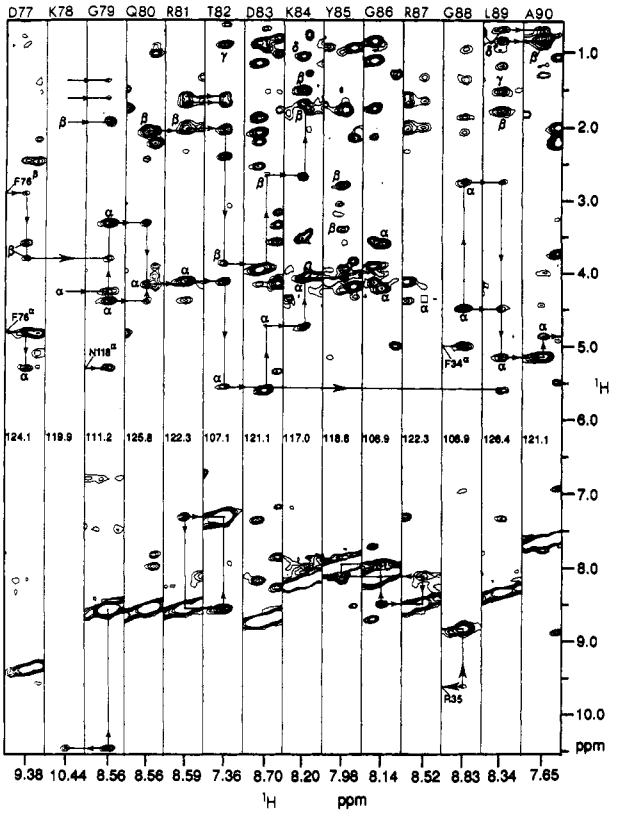


FIGURE 10: 3D $^1H$–$^{15}N$ NOESY-HMQC data that identify the presence of the D77–A90 loop and characterize its structure. The 14 $^1H$–$^1H^N$ strips are arranged in sequential order. The NOE connectivities between protons of residues in this loop are denoted by solid lines. The notation used in the figure is defined in the legend to Figure 3.

turn as determined by a series of three rectangular $d_{NN}$ NOE connectivities between the $^1H^N$'s of I139, W140, S141, and E142. An additional NOE connects the $^1H^\alpha$ of L137 with the $^1H^N$ of D143 (Figure 3S).

### *Long-Range NOE Connectivities and Side-Chain Assignments*

A number of long-range NOE connectivities were observed in the 3D $^1H$–$^{15}N$ NOESY-HMQC spectrum of nuclease H124L. In Figure 8, the G20 strip shows three interresidue NOE cross peaks that serve to connect the $^1H^N$ of G20 to the $^1H^\alpha$ of S59 and the two $^1H^\beta$'s of Y113. This places the $\alpha$-helical turn of the second $\beta$-sheet close in space to the N-terminus of the A58–A69 $\alpha$-helix. The side chain of Y113, which is located in the small loop, extends toward the I18–T22 $\alpha$-helical turn.

Long-range connectivities (Figure 10) are observed between the $^1H^\alpha$'s of F34 and N118 and the $^1H^N$'s of G88 and G79, respectively, and between the $^1H^N$'s of G88 and R35. These three NOE's place the N-terminus of the big loop close in space to the small loop and the C-terminus of the big loop close to the C-terminus of the P31–R35 strand of the second $\beta$-sheet.

We were able to identify side-chain proton resonances from several lysines and leucines in the 3D NMR spectrum by reference to $^1H$ 2D COSY cross peaks (Wang et al., 1992). These side-chain assignments are noted in the strips corresponding to these residues. The $^1H^\beta$ resonances of L7, L36, and L38 were not found. Additional long-range (tertiary) NOE connectivities observed in the 3D NMR spectrum are indicated in the figures in which they appear.

## CONCLUSION

We have described in detail the spectral assignments and elucidation of secondary structure of uncomplexed nuclease H124L as derived from 3D $^1H$–$^{15}N$ NOESY-HMQC data. The assigned 3D connectivity patterns provide an excellent overview of the secondary structure of the protein. A long series of rectangles indicates $d_{NN}$ NOE connectivities characteristic of a stretch of $\alpha$-helix. A pattern of discrete rectangles that correspond to NOE's between residues of adjacent strands indicates the presence of antiparallel $\beta$-sheet. Discrete rectangles that link strips within a four-residue segment indicate the presence of a turn in the $\beta$-sheet.

The sequential assignments of $^1H$ and $^{15}N$ resonances from residues within $\alpha$-helices were easily determined from the patterns of symmetry-related NOE cross peaks in the 3D spectrum. Assignments in $\alpha$-helical stretches were extended sequentially into other structural domains by means of $d_{\alpha N}$ connectivities. Additional interresidue NOE connectivities in the 3D spectrum, such as those between $^1H^N$'s and $^1H^\delta$'s or $^1H^\gamma$'s, provided tertiary structural information. The present results as extended by the 2D NMR data (Wang et al., 1992) lay the groundwork for full three-dimensional solution structural analysis of this protein (work in progress).

## ACKNOWLEDGMENTS

We thank Dr. W. Milo Westler for supplying the W2FFT routine used for the $\omega_2$ Fourier transformation of the 3D data.

## Supplementary Material Available

Figure 1S showing four $^1H$–$^1H^N$ strips that represent NOE cross peaks from the A69–I72 segment; Figure 2S showing six $^1H$–$^1H^N$ strips with NOE connectivities that characterize the structure of the loop in the Y113–N119 segment; Figure 3S showing six $^1H$–$^1H^N$ strips with NOE's that define an $\alpha$-helical turn in the N138–D143 segment (4 pages). Ordering information is given on any current masthead page.

**Registry No.** Staphylococcal nuclease, 9013-53-0.

## References


Clore, G. M., Bax, A., Driscoll, P. C., Wingfield, P. T., & Gronenborn, A. M. (1990a) *Biochemistry 29*, 8172–8184.

Clore, G. M., Bax, A., Wingfield, P. T., & Gronenborn, A. M. (1990b) *Biochemistry 29*, 5671–5676.

Driscoll, P. C., Clore, G. M., Marion, D., Wingfield, P. T., & Gronenborn, A. M. (1990a) *Biochemistry 29*, 3542–3556.

Driscoll, P. C., Gronenborn, A. M., Wingfield, P. T., & Clore, G. M. (1990b) *Biochemistry 29*, 4668–4682.

Englander, S. W., & Wand, A. J. (1987) *Biochemistry 26*, 5953–5958.

Fesik, S. W., & Zuiderweg, E. R. P. (1990) *Q. Rev. Biophys. 23*, 97–131.

Fesik, S. W., Eaton, H. C., Olejniczak, E. T., & Zuiderweg, E. R. P. (1990) *J. Am. Chem. Soc. 112*, 886–888.

Ikura, M., Kay, L. E., & Bax, A. (1990a) *Biochemistry 29*, 4659–4667.

Ikura, M., Bax, A., Clore, G. M., & Gronenborn, A. M. (1990b) *J. Am. Chem. Soc. 112*, 9020–9022.

Kay, L. E., Marion, D., & Bax, A. (1989) *J. Magn. Reson. 84*, 72–84.

Kay, L. E., Ikura, M., & Bax, A. (1991) *J. Magn. Reson. 91*, 84–92, and references therein.

Marion, D., Driscoll, P. C., Kay, L. E., Wingfield, P. T., Bax, A., Gronenborn, A. M., & Clore, G. M. (1989a) *Biochemistry 28*, 6150–6156.

Marion, D., Kay, L. E., Sparks, S. W., Torchia, D. A., & Bax, A. (1989b) *J. Am. Chem. Soc. 111*, 1515–1517.

Marion, D., Ikura, M., Tschudin, R., & Bax, A. (1989c) *J. Magn. Reson. 85*, 393–399.

Markley, J. L., & Jardetzky, O. (1970) *J. Mol. Biol. 50*, 223–233.

Markley, J. L., Darba, P., Fejzo, J., Krezel, A. M., Macura, S., McNemar, C. W., Mooberry, E. S., Westler, W. M., & Zolnai, Z. (1991) *Proceedings of the NATO Workshop on Computational Aspects of the Study of Biological Macromolecules* (Hoch, J. C., Ed.) pp 39–50, NATO ASI Series, Plenum Press, New York.

Morris, G. A., & Freeman, R. (1978) *J. Magn. Reson. 29*, 433–462.

Shon, K., & Opella, S. J. (1989) *J. Magn. Reson. 82*, 193–197.

Simorre, J., & Marion, D. (1990) *J. Magn. Reson. 89*, 191–197.

States, D. J., Haberkorn, R. A., & Ruben, D. J. (1982) *J. Magn. Reson. 48*, 286–292.

Torchia, D. A., Sparks, S. W., & Bax, A. (1989) *Biochemistry 28*, 5509–5524.

Ulrich, E. L., Markley, J. L., & Kyogoku, Y. (1989) *Protein Sequences Data Anal. 2*, 23–37.

Wagner, G., Neuhaus, D., Wörgötter, E., Vasák, M., Kägi, J. H. R., & Wüthrich, K. (1986) *J. Mol. Biol. 187*, 131–135.

Wand, A. J., & Englander, S. W. (1986) *Biochemistry 25*, 1100–1106.

Wang, J., Hinck, A. P., Loh, S. N., & Markley, J. L. (1990a) *Biochemistry 29*, 102–113.

Wang, J., LeMaster, D. M., & Markley, J. L. (1990b) *Biochemistry 29*, 88–101.

Wang, J., Hinck, A. P., Loh, S. N., LeMaster, D. M., & Markley, J. L. (1992) *Biochemistry* (following paper in this issue).

Zolnai, Z., Westler, W. M., Ulrich, E. L., & Markley, J. L. (1990) *J. Magn. Reson. 88*, 511–522.

Zuiderweg, E. R. P., & Fesik, S. W. (1989) *Biochemistry 28*, 2387–2391.

Zuiderweg, E. R. P., McIntosh, L. P., Dahlquist, F. W., & Fesik, S. W. (1990) *J. Magn. Reson. 86*, 210–216.